Floquet exponents of underdamped Josephson ladders: A comparison with predictions of the discrete sine-Gordon equation

B. R. Trees and N. Hussain*
Department of Physics and Astronomy, Ohio Wesleyan University, Delaware, Ohio 43015
(Received 6 August 1999; revised manuscript received 15 March 2000)

We calculate Floquet exponents for phase-locked solutions in ladder arrays of Josephson junctions in zero external field. We assume a resistively and capacitively shunted junction (RCSJ) model, and we allow for critical current anisotropy between the horizontal and vertical junctions. The ladders range in size from 5 to 30 plaquettes and are biased along the rungs with uniform dc bias currents. The Floquet exponents quantify the stability of the solutions and are calculated numerically for the RCSJ model as a function of junction capacitance (β_c) as well as critical current anisotropy (Λ). We also model the array with the discrete sine-Gordon (DSG) equation, and we are able to calculate the exponents analytically in that case. We find the analytic results from the DSG equation agree quantitatively with the numerical results from the RCSJ model over a wide range of β_c and Λ values and even agree qualitatively for $\beta_c \to 1$ and $\Lambda \to 0$. Based on the analytic result we argue that perturbations in the array are damped by the small-angle phase oscillations of the underlying lattice (the ''phonons'' of the lattice), and like a classical harmonic oscillator with damping, each phonon mode has a crossover (as a function of decreasing β_c or Λ) from underdamped to overdamped dynamics. Such crossover behavior is clearly visible in the results for the Floquet exponents and is manifested as a maximum in the Floquet exponent as a function of the junction capacitance. This intriguing result speaks to the opportunity, in principle, of tuning the capacitance such as to optimize the stability of the phase-locked solutions.

PACS number(s): 74.50.+r, 05.45.−a, 05.45.Xt, 74.60.Jg

I. INTRODUCTION

Over the last decade there has existed considerable interest in the dynamics of ladder arrays and the similar but not identical parallel arrays of Josephson junctions. Both experimental and theoretical work has been done by many [1–18] in an attempt to understand the rich behavior such nonlinear systems can exhibit. One factor leading to interest in these geometries has been that they are excellent examples of real-world systems that can, under appropriate conditions, be modeled by the discrete sine-Gordon equation [4,11,12,14,15,19–22]. As part of this work, we have been studying the so-called whirling mode solutions to the discrete sine-Gordon equation. It is easy to understand how the adjective ''whirling'' is appropriate when one considers a common mechanical analog of a Josephson junction array, namely a damped, driven set of pendula with nearest neighbors connected by torsional springs. In such a system one quantity of importance is the angle of the pendulum's rotation ϕ, and the whirling mode describes the situation in which the driving torque on the pendula is large enough (in the presence of gravity) to allow them to execute complete rotations about their supports. It turns out that the simple equation $\phi = \omega t$ then describes a particular pendulum's angular displacement with respect to time, where ω is an angular velocity. In the language of the original Josephson junctions, this behavior occurs when the bias current driving the array is greater than a typical junction's critical current. The stability of such a solution will be part of the focus of this paper.

In generic terms the discrete sine-Gordon (DSG) equation describes a system of damped, driven particles that are connected to their nearest neighbors by springs and that also experience a sinusoidal external potential [23,24]. One of its original manifestations was in studies of dislocations in crystals and in that context (zero damping and zero driving force) it is known as the Frenkel-Kontorova model [25]. For describing underdamped Josephson junctions [26], a common model of choice is the resistively and capacitively shunted junction (RCSJ) model [27]. It has been argued that the RCSJ model is equivalent to the DSG equation in the limit of small spatial variations of the superconducting Josephson phase differences along the ladder [4,12]. As a result of this condition on the phase variations it is not surprising that most previous work with the DSG equation as applied to Josephson ladders and parallel arrays has focused on the highly underdamped limit, corresponding to McCumber parameters ($\beta_c = 2eI_cR^2C/\hbar$, where I_c, R, C are a junction's critical current, resistance, and capacitance, respectively) of approximately 50 or greater [4,11,13,14,20,21]. Nevertheless, it is natural to ask how well the DSG equation describes the dynamics of the RCSJ model, well known for being an accurate predictor of the behavior of actual arrays of Josephson junctions over a wide range of parameters, for smaller values of β_c, for example for $\beta_c \lesssim 20$.

In this paper we report on a comparison of the dynamics of the DSG equation with that of the RCSJ model for a ladder array of underdamped Josephson junctions in the whirling regime and for McCumber parameters in the range $1 < \beta_c \lesssim 40$. Specifically, our geometry is shown in Fig. 1. The junctions parallel to the x axis (the horizontal junctions) have a critical current I_{cx}, while the vertical junctions (parallel to the y axis) have a critical current I_{cy}. All other junc-

*Present address: Washington University, St. Louis, MO 63130-4899.

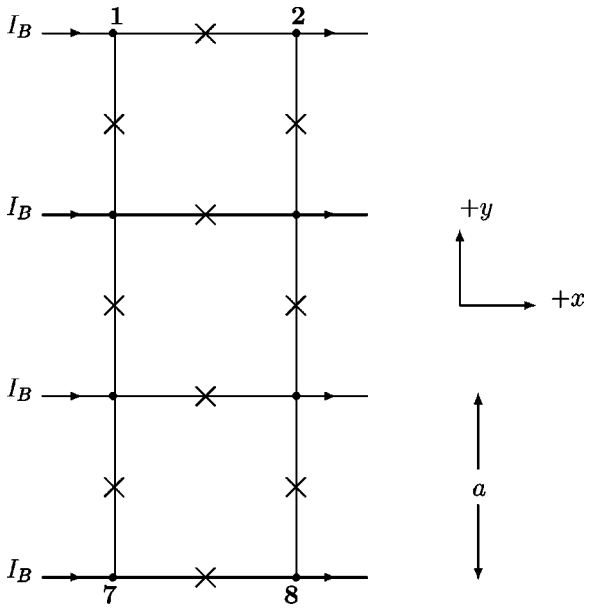

FIG. 1. Geometry of the ladder array of Josephson junctions. The horizontal junctions, along the rungs of the ladder, are parallel to the *x* axis, while the vertical junctions are parallel to the *y* axis. This figure depicts a ladder with $N=3$ cells and eight nodes, four of which are explicitly labeled. A dc bias current, I_B, is injected at each node on the left side and extracted from the right side. *a* denotes the dimension of each cell. We assume periodic boundary conditions along the long direction of the ladder, so that in this figure nodes 1 and 7 (and 2 and 8) are actually the same.

tions parameters, e.g., resistance (R) and capacitance (C), are assumed identical. A spatially uniform, dc bias current I_B is fed into the horizontal junctions on the left and extracted from the right side. The long direction of the ladder (the *y* direction) is constrained by periodic boundary conditions. The number of cells (plaquettes) of the ladder is denoted by N; typically we have studied ladders with N ranging from 5 to 30.

We consider phase-locked solutions for the horizontal junctions, by which we mean a solution in which the horizontal junctions have identical voltage versus time plots. Our numerical algorithm initializes the superconducting phases at the nodes of the ladder randomly, and it is easily determined that the voltages, which are periodic in time, have indeed synchronized, i.e., phase locked, within a relatively few periods. To test the stability of phase-locking to mechanical perturbations, we calculate the Floquet exponents (see Sec. II) for these solutions. We do so both numerically for the RCSJ model and analytically for the DSG equation. For the ladder sizes considered in detail ($N=10$, 15, 20, and 25) the exponents calculated for the two models agree quantitatively for $\beta_c \gtrsim 10$, and perhaps surprisingly, agree at least qualitatively even for smaller β_c (see Fig. 7). The results also show a possibility of ''tuning'' the stability of phase locking in the array in that the minimum Floquet exponent clearly shows nonmonotonic behavior for decreasing β_c with a peak (signifying the most stable phase locking) occuring at a certain ''crossover'' point, $\beta_c^*(N)$, that is a function of array size. Furthermore, the analytic result for the Floquet exponents (from the DSG equation) gives us a physical picture to describe, at least partially, the dynamics of the ladder responsible for the phase locking. The organization of the remainder of this paper is as follows. In Sec. II we describe the numerical calculation of the Floquet exponents as based on the RCSJ model. Section III describes the dynamics of the discrete sine-Gordon equation in more detail and discusses the analytic calculation of the Floquet exponents from the equation. Finally, in Sec. IV we compare and contrast the results for the exponents from the two models.

II. RCSJ MODEL

It is expedient to use a system of dimensionless variables for the subsequent calculations. Let the characteristic time scale for a junction be $t_c \equiv \hbar/2eI_{cx}R$, so that we can define a dimensionless time variable, $\tau \equiv t/t_c$. The dimensionless dc bias current entering or leaving node j is $i_{B,j} \equiv I_{B,j}/I_{cx}$. Referring to Fig. 1, conservation of the charge at the jth node yields

$$i_{B,j} + \sum_{\langle k \rangle} \left[i_{c,jk} \sin(\theta_j - \theta_k) + \frac{d}{d\tau}(\theta_j - \theta_k) + \beta_c \frac{d^2}{d\tau^2}(\theta_j - \theta_k) \right] = 0. \tag{1}$$

Here θ_j is the superconducting phase at node j, and $i_{c,jk} \equiv I_{c,jk}/I_{cx}$ is the dimensionless critical current of the junction between nodes j and k. The sum runs over all nearest-neighbor nodes to j. We allow for critical current anisotropy in that I_{cx} and I_{cy} need not be equal. In fact we will define a measure of the critical current anisotropy as $\Lambda^2 \equiv I_{cy}/2I_{cx}$. The McCumber parameter β_c was defined in Sec. I. The array is not subjected to any external magnetic field. Equation (1) is combined with the standard Josephson voltage expression for node j,

$$V_j = \frac{\hbar}{2e}\frac{d\theta_j}{dt},$$

which if we define a characteristic voltage $V_c \equiv I_{cx}R$, can be written in dimensionless form

$$v_j \equiv \frac{V_j}{V_c} = \frac{d\theta_j}{d\tau}. \tag{2}$$

We have solved Eqs. (1) and (2) numerically using the fourth-order Runge-Kutta method, with (dimensionless) time steps of $\Delta\tau = 0.001$. Typically, the code was run for at least a time of $\tau_{total} = 400$ to allow the horizontal junctions to phase lock. Then the Floquet (stability) analysis was performed, which we now describe.

Suppose that $\theta_{0j}(\tau)$ is a solution to Eqs. (1) and (2). We perturb the phase at node j by an amount $\eta_j(\tau)$ so that the new phase is $\theta_j(\tau) = \theta_{0j}(\tau) + \eta_j(\tau)$. Linearizing Eq. (1) with respect to η_j, we arrive at the following:

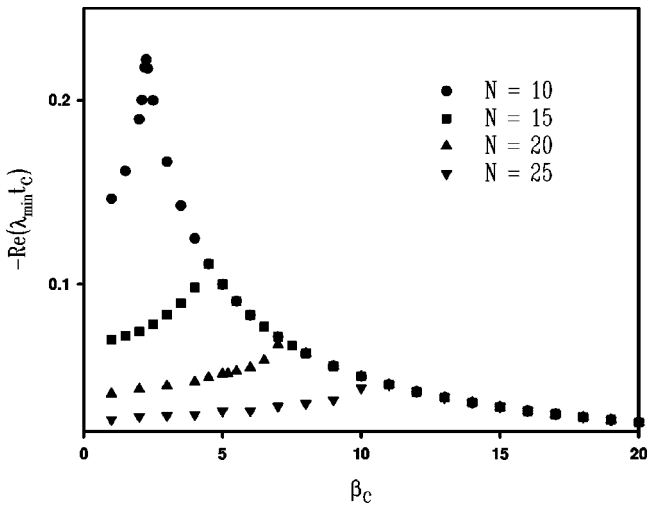

FIG. 2. Magnitude of the minimum Floquet exponent versus the McCumber parameter for four different ladder sizes. The bias current was fixed at $i_B=10$, and the critical current anisotropy was $\Lambda=1/\sqrt{2}$. The exponent shows nonmonotonic behavior as a function of β_c, with a maximum at $\beta_c^*(N)$, which is a function of ladder size. The value of $\beta_c^*(N)$ marks a crossover from underdamped $[\beta_c>\beta_c^*(N)]$ to overdamped behavior $[\beta_c<\beta_c^*(N)]$.

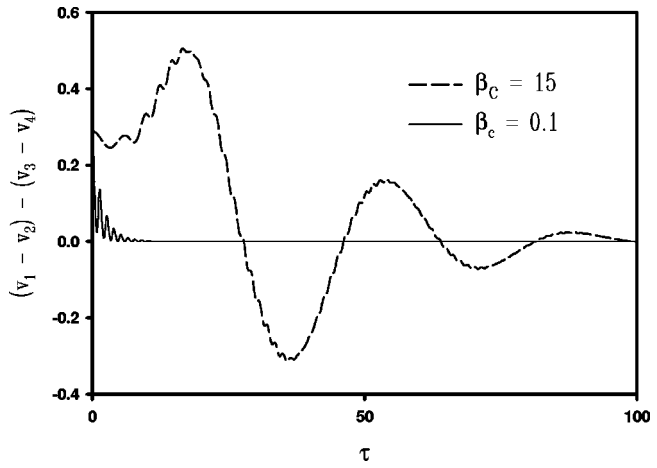

FIG. 3. Difference of the voltages across the top two junctions of an $N=5$ ladder as a function of time for two different values of β_c. The bias current was $i_B=5$, and the critical current anisotropy was $\Lambda=1/\sqrt{2}$. All voltages are initially randomized. In the large β_c case ($\beta_c=15$) the approach to phase locking shows characteristic underdamped behavior, while for $\beta_c=0.1$, the decay of the signal appears to be overdamped. In both cases, the signals also exhibit a ''high frequency'' oscillatory behavior with which we are not interested.

$$\sum_{\langle k \rangle} \left[i_{c,jk} \cos(\theta_{0j}-\theta_{0k})(\eta_j-\eta_k) + \frac{d}{d\tau}(\eta_j-\eta_k) + \beta_c \frac{d^2}{d\tau^2}(\eta_j-\eta_k) \right] = 0. \tag{3}$$

Because the coefficients of the η_j are periodic, with period T/t_c in dimensionless units, we can apply Floquet's theorem [28], which tells us that there exist solutions to Eq. (3) of the form

$$\eta_j\left(\tau+\frac{T}{t_c}\right)=\mu\,\eta_j(\tau), \tag{4}$$

where μ is a (possibly complex) number called the Floquet multiplier. We are interested in the case when $|\mu|<1$, which corresponds to perturbations that diminish with time. Of course, $|\mu|>1$ denotes instability in that perturbations grow over time, and the special case of $|\mu|=1$ is called neutral stability. There is a corresponding Floquet exponent, λ, which is related to the Floquet multiplier by

$$\mu=e^{\lambda T}=e^{(\lambda t_c)(T/t_c)}. \tag{5}$$

The condition $|\mu|<1$ corresponds to $\mathrm{Re}(\lambda)<0$. We can think physically of the exponents (or multipliers) as describing the stability of the characteristic modes of the array. *At least* one of these exponents must equal zero, which is a result of the invariance of Eq. (1) to a time translation. Excluding the exponent of zero, we are interested in the remaining exponent of *smallest magnitude*, $|\lambda_{min}|$, as that tells us by what factor the longest-lived mode of the array decays (or grows) in one period after a perturbation [29].

We have performed a stability analysis for ladders of size $N=10$, 15, 20, and 25 with $1<\beta_c\lesssim 40$ and bias currents from about $2I_{cx}$ to $20I_{cx}$. Consider Fig. 2, which shows $-\mathrm{Re}(\lambda_{min}t_c)$ versus β_c for $i_B=10$, $\Lambda=1/\sqrt{2}$ (corresponding to $I_{cx}=I_{cy}$) and several values of N. There is a general trend for decreasing β_c of increasing stability (as demonstrated by a growing magnitude of the Floquet exponent) down to a crossover value of the McCumber parameter, $\beta_c^*(N)$, which is dependent upon ladder size. For decreasing β_c below $\beta_c^*(N)$, the phase locking takes increasingly longer to recover from a mechanical perturbation. As is clearly seen from the figure, this crossover behavior of the stability is a sharp function of β_c. Furthermore, above the crossover $[\beta_c>\beta_c^*(N)]$, the Floquet exponent has a simple form, namely $\mathrm{Re}(\lambda_{min}t_c)=-1/2\beta_c$, which holds for all the ladder sizes and bias currents we have looked at (as long as the ladder is in the whirling regime, of course).

The peak in the exponent, observed in Fig. 2 for a given ladder size, implies behavior similar to that of a classical damped oscillator, in which the case of critical damping gives the largest decay constant compared to both the underdamped and overdamped cases. This comparison with a damped oscillator is worthy of elaboration. It is well known [30] that the solution for the position as a function of time of a classical, damped harmonic oscillator in the absence of a driving force decays most rapidly when the damping parameter (representing the amount of friction in the system) is tuned to the special value corresponding to critical damping. If one were to plot the decay rate of the solutions for this system (i.e., the coefficient of the time variable in the argument of the exponential) as a function of the inverse of the damping parameter one would observe a peak in the decay rate for the case of critical damping. We are arguing that the peak observed in Fig. 2 for a given N is analogous to this classical behavior. Furthermore, the comparison of our system with classical damped oscillators is strengthened by Fig. 3, which plots the *difference* of the voltages across the top two horizontal junctions in a ladder with $N=5$, $i_B=5$, and

TABLE I. The Floquet exponents obtained from a numerical solution of Eq. (3) for a ladder with $N=5$, $i_B=10$, and $\Lambda=1/\sqrt{2}$. There are 18 characteristic modes of such an array, each mode having a corresponding Floquet exponent. The exponents for $\beta_c=1.1$ (underdamped regime) and $\beta_c=0.7$ (overdamped regime) are shown.

$\mathrm{Re}(\lambda t_c)$ for $\beta_c=1.1$	$\mathrm{Re}(\lambda t_c)$ for $\beta_c=0.7$
0.0004	−0.0003
−0.4543	−0.5432
−0.4543	−0.7139
−0.4543	−0.7139
−0.4543	−0.7139
−0.4543	−0.7139
−0.4543	−0.7139
−0.4543	−0.7139
−0.4543	−0.7139
−0.4543	−0.7139
−0.4543	−0.7139
−0.4543	−0.7139
−0.4547	−0.7139
−0.4547	−0.7143
−0.4735	−0.7143
−0.4735	−0.7361
−0.4900	−0.7361
−0.4900	−0.9631
−1.4392	−2.3104

$\Lambda=1/\sqrt{2}$. The characteristic shapes of the two curves are clearly reminiscent of underdamped ($\beta_c=15$) and overdamped ($\beta_c=0.1$) behavior with some ''high'' frequency oscillations superimposed. Also, the nonmonoticity of the exponent's dependence on β_c seen in Fig. 2 suggests, at least in principle, the possibility of tuning the value of β_c to control the degree of stability of the array.

To offer the reader a better feeling for the numerical results obtained in our stability analysis, we include a table of *all* the Floquet exponents calculated for an array with $N=5$, $i_B=10$, $\Lambda=1/\sqrt{2}$ and two different values of β_c. The details of the numerical procedure used to calculate the exponents is essentially the same as that described elsewhere [31]. For a ladder with N cells and periodic boundary conditions, there are $2(2N-1)$ coupled first-order differential equations to be solved numerically. Correspondingly, there are $2(2N-1)$ Floquet exponents for a given set of circuit parameters. The first column of Table I shows all 18 exponents of a five cell ladder with $\beta_c=1.1$, which satisfies the condition $\beta_c>\beta_c^*(5)$. We see there is one exponent approximately equal to zero, as expected and as explained above. We also note the exponent with a value of $-1/2\beta_c$ has a high degree of degeneracy. The second column shows all exponents for $\beta_c=0.7$, which corresponds to $\beta_c<\beta_c^*(5)$. Other than the exponent of (approximately) zero and the highly degenerate exponent of $-1/2\beta_c$, we also note the appearance of a single exponent of magnitude less than $1/2\beta_c$. This signals the crossover from underdamping to overdamping has occured.

In Fig. 4, which plots $-\mathrm{Re}(\lambda_{min}t_c)$ versus β_c for $N=15$ and $\Lambda=1/\sqrt{2}$, we see that the minimum Floquet exponent is independent of bias current over a wide range of currents. There is some observable deviation for small β_c for $i_B=2$, presumably because of the proximity of the boundary to the whirling regime (i.e., we are near $i_B=1$). We see similar behavior for other size ladders. Figure 5 shows the dependence of the minimum Floquet exponent on the critical current anisotropy Λ for three different ladder sizes. All results are for $i_B=10$ and $\beta_c=20$. Here the dependence on anisotropy is flat for Λ greater than some crossover value that is dependent on ladder size, $\Lambda^*(N)$, and then the exponents drop rather sharply towards zero. For $\Lambda>\Lambda^*(N)$ we have the typical underdamped result that $\mathrm{Re}(\lambda_{min}t_c)=-1/2\beta_c$, independent of N and i_B for all values of those parameters that we have tried. The fact that $-\mathrm{Re}(\lambda_{min}t_c)\to 0$ for sufficiently small Λ is easy to understand. As we shall see in the context of the DSG equation, Λ is also a measure of the coupling between a horizontal junction and

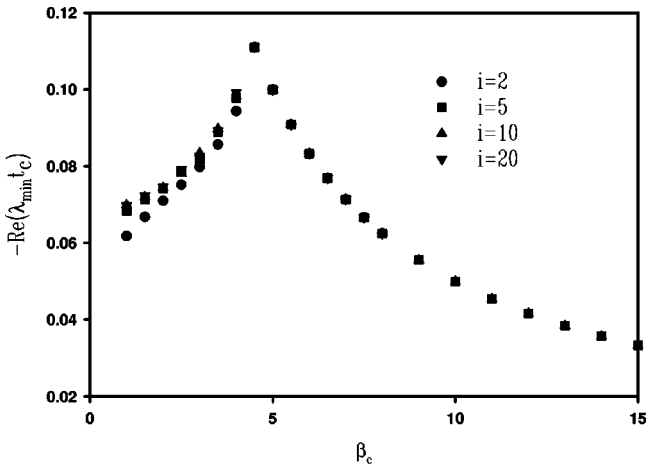

FIG. 4. Magnitude of the minimum Floquet exponent versus the McCumber parameter for an $N=15$ ladder and for four different dc bias currents. The critical current anisotropy was $\Lambda=1/\sqrt{2}$. Except for $i_B=2$ in the region $\beta_c\leqslant 2$, the exponents are independent of the bias current.

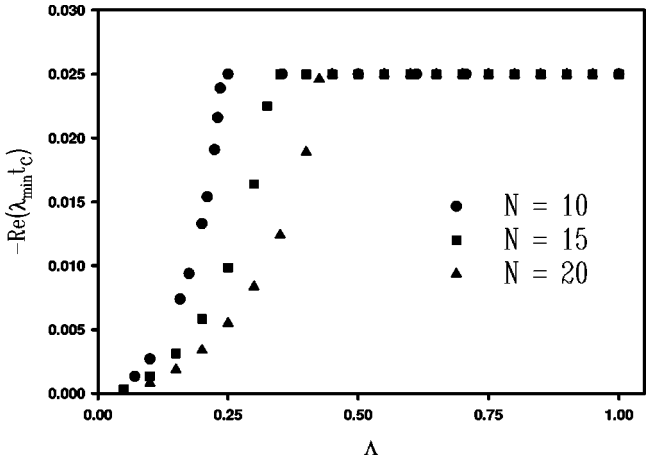

FIG. 5. Magnitude of the minimum Floquet exponent versus critical current anisotropy for three different sized ladders. The McCumber parameter was $\beta_c=20$ and the dc bias current was $i_B=10$. The exponent equals $-1/2\beta_c$ independent of N and Λ for Λ greater than some crossover value, $\Lambda^*(N)$, which is dependent on ladder size. For $\Lambda<\Lambda^*(N)$, the exponents quickly drop towards zero.

its nearest-neighbor horizontal junctions. As Λ gets small we are approaching a limit of N independent junctions. In that case, a mechanical perturbation applied to a given junction cannot decay by in turn perturbing a neighboring junction and thereby propagating along the ladder. Thus, as is generally the case with a set of independent oscillators, we expect to see evidence of neutral stability ($\lambda_{min} \rightarrow 0$), which is indeed the observed behavior.

III. DISCRETE SINE-GORDON EQUATION

Kardar [12] first introduced the ladder of anisotropic Josephson junctions as a system whose dynamics could be modeled by the discrete sine-Gordon equation. Since then, several groups have worked on the dynamics of the DSG equation as applied to ladder arrays and parallel arrays [4,11,14,15,20,21]. For example, van der Zant and collaborators [13,14] fabricated and studied so-called ring arrays, which are examples of parallel arrays that are similar but not identical to ladders [32]. With an eight cell ring, $\Lambda^2 \approx 3$, and $\beta_c \approx 50$, they measured resonance steps in the *IV* characteristics of their arrays. They were able to explain the steps within the context of the DSG equation by focusing on so-called parametric instabilities of the system, in which the whirling modes can become unstable by exciting ''phonons'' [33] in a kind of positive feedback loop. By contrast, the values of i_B, β_c, and Λ used in our simulations do not place us near to such instabilities (see Sec. IV).

We wish to see how well our numerical results for the Floquet exponents for Josephson ladders, based on the RCSJ model, are in agreement with what the DSG equation yields. It is important to understand that agreement between the two models is expected to breakdown as β_c is decreased sufficiently, since (as we approach the overdamped limit, $\beta_c \rightarrow 0$) the Josephson phase differences across horizontal junctions can vary appreciably along the ladder. The physics of this statement is worth discussing. To do so, it is useful to change slightly how we label the junctions in the array. Now, let j index only the *horizontal* junctions (along the rungs of the ladder), and let ϕ_j represent the superconducting phase *difference* across the jth junction, that is, using the notation of Fig. 1, $\phi_1 = \theta_1 - \theta_2$. Consider Fig. 6, which plots the *difference* of the phase differences across junctions one and two, $\phi_1 - \phi_2$, and the same quantity for junctions six and seven, $\phi_6 - \phi_7$, versus time for a ten cell ladder. At $\tau = 200$, the phase difference ϕ_1 is mechanically perturbed, and by looking at the two plots, $\phi_1 - \phi_2$ and $\phi_6 - \phi_7$, we can get a feeling for how the perturbation travels along the ladder. In Fig. 6(a), which is calculated for $\beta_c = 100$, there is clearly a time lag for the perturbation to reach junctions six and seven, but the disturbance still has a measurable amplitude when it does reach those junctions. In Fig. 6(b), which corresponds to $\beta_c = 1$, we see that the disturbance is essentially completely damped before reaching junctions six and seven. (Also note the different time scales of the two graphs.) Clearly, Fig. 6(b) shows a large variation between the behavior of junctions one and six, for example. It is this spatial variation, evident for small β_c, that we expect the DSG equation to be unable to describe quantitatively. Nevertheless, we claim the DSG equation may still be useful to consider even for $\beta_c \approx 1$, since it offers us more of a physically

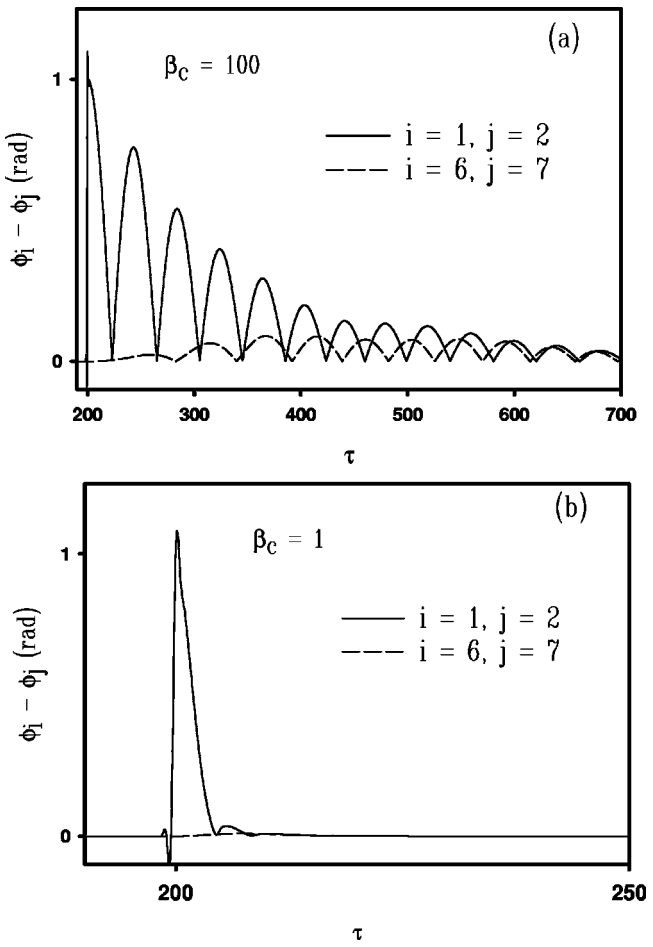

FIG. 6. *Difference* in the superconducting phase difference between neighboring horizontal junctions versus time for an $N = 10$ ladder with $i_B = 10$ and $\Lambda = 1/\sqrt{2}$. In both plots, the phase difference across the first junction ϕ_1 was mechanically perturbed at $\tau = 200$. (a) The difference between the phase differences for the first and second, and sixth and seventh, junctions are shown for $\beta_c = 100$. We see that the perturbation travels from the first junction to the sixth and seventh junctions in a time interval of roughly $\Delta\tau \approx 300$, and that the amplitude of the perturbation still has measurable size by the time the sixth junction is reached. (b) The same difference as in (a) is plotted, but now for $\beta_c = 1$. We see that a perturbation created at the first junction has no appreciable magnitude at the sixth junction during any time. [The data were calculated for plot (b) for τ up to 700, but the scale of the horizontal axis is as shown, since the only time interval where junction six shows any disturbance at all is for τ near 210.]

intuitive picture of the dynamics than does the RCSJ model. The details of the analytic calculation of the Floquet exponents from the DSG equation follow.

In the context of the DSG equation, the role of the vertical junctions is to provide the coupling for a given horizontal junction with its nearest-neighbor horizontal junctions [34]. It turns out that the strength of this coupling is measured by the quantity $\Lambda^2 = I_{cy}/2I_{cx}$, where Λ is the same critical current anisotropy parameter defined in Sec. I. Using our new labeling scheme for the horizontal junctions, the DSG equation takes the following form in dimensionless units:

$$\beta_c \frac{d^2\phi_j}{d\tau^2} + \frac{d\phi_j}{d\tau} + \sin(\phi_j) - \Lambda^2 \nabla^2 \phi_j + i_B = 0, \qquad (6)$$

where $\nabla^2\phi_j=\phi_{j+1}-2\phi_j+\phi_{j-1}$ is the discrete Laplacian and where all distances are measured in terms of the cell size a (see Fig. 1).

A stability analysis of Eq. (6) leads to the damped Mathieu equation, as shown by Watanabe and co-workers [14,20,21]. One lets $\phi_i=\phi_{0j}+\eta_j$ and linearizes the DSG equation with respect to η_j. The result is

$$\beta_c\frac{d^2\eta_j}{d\tau^2}+\frac{d\eta_j}{d\tau}+[\cos(\phi_{0j})]\eta_j-\Lambda^2\nabla^2\eta_j=0. \tag{7}$$

Since we are interested in the whirling regime we consider $i_B>1$. Then the junction voltages have a well defined period T and, as can be verified from the numerics, we can write the unperturbed phase differences as

$$\phi_{0j}=\left(\frac{2\pi}{T}\right)t=\left(\frac{2\pi}{T/t_c}\right)\left(\frac{t}{t_c}\right)\equiv\omega\tau,$$

where ω is a dimensionless angular frequency. Next, we assume periodic boundary conditions, $\eta_{j+N}=\eta_j$, and we expand the perturbations as a Fourier series,

$$\eta_j(\tau)=\sum_{m=0}^{N-1}A_m(\tau)e^{2\pi imj/N}.$$

When this expression is substituted into Eq. (7), the Fourier modes decouple and we have

$$\beta_c\frac{d^2A_m}{d\tau^2}+\frac{dA_m}{d\tau}+\left[4\Lambda^2\sin^2\left(\frac{\pi m}{N}\right)+\cos(\omega\tau)\right]A_m=0. \tag{8}$$

It is common to make the definition $\omega_m^2\equiv4\Lambda^2\sin^2(\pi m/N)$, where we can think of the ω_m as frequencies of small amplitude oscillations of an analogous pendulum system (the so-called ''phonon'' frequencies, or normal mode frequencies). To simplify a comparison of Eq. (8) with the standard Mathieu equation, let $\tau'\equiv\omega\tau$; then, after dividing through by β_c we arrive at

$$\frac{d^2A_m}{d\tau'^2}+\frac{1}{\omega\beta_c}\frac{dA_m}{d\tau'}+\left[\frac{\omega_m^2+\cos\tau'}{\beta_c\omega^2}\right]A_m=0. \tag{9}$$

Next, we define a set of dimensionless quantities, $\kappa\equiv1/\omega\beta_c$, $\nu_m\equiv\omega_m^2/\omega^2\beta_c$, and $\gamma\equiv1/\omega^2\beta_c$. Note that for the our simulations of the whirling regime, we have $\omega>1$ (see below). Also note that as long as the coupling parameter, Λ, is not much larger than one and the system is highly underdamped ($\beta_c\gg1$), all three of these quantities (κ, ν_m, and γ) are small.

At this point we make the standard transformation

$$A_m(\tau')=e^{-\kappa\tau'/2}\rho_m(\tau'), \tag{10}$$

which introduces the new function $\rho_m(\tau')$. Equation (9) then becomes

$$\frac{d^2\rho_m}{d\tau'^2}+\left[\nu_m-\frac{\kappa^2}{4}+\gamma\cos\tau'\right]\rho_m=0, \tag{11}$$

which has the standard form of a Mathieu equation. Note that this equation can be written in the general form

$$\frac{d\mathbf{X}}{d\tau'}=\mathbf{P}(\tau')\mathbf{X}, \tag{12}$$

where

$$\mathbf{X}=\begin{pmatrix}\dfrac{d\rho_m}{d\tau'}\\ \rho_m\end{pmatrix}$$

and where the 2×2 matrix $\mathbf{P}(\tau')$ is periodic with a minimal period of 2π. From Floquet's theorem [28] we know there are solutions to Eq. (11) of the form

$$\rho_m(\tau')=e^{(\overline{\lambda}_m t_c)\tau'}Q_m(\tau'), \tag{13}$$

where $Q_m(\tau')$ is a periodic function with the same period as the coefficient matrix $\mathbf{P}(\tau')$, namely 2π, and $(\overline{\lambda_m t_c})$ is the Floquet exponent for the solutions ρ_m. [Note the similarity of the argument of the exponential to that in Eq. (5). Also note the overbar notation is merely to indicate the Floquet exponents of the ''intermediate'' functions $\rho_m(\tau')$]. We want a solution for the Fourier coefficients $A_m(\tau')$ that corresponds to Eq. (13). Based on Eq. (10) such a solution would be

$$A_m(\tau')=e^{(\overline{\lambda_m}t_c-\kappa/2)\tau'}Q_m(\tau').$$

After restoring the original time variable, $\tau=\tau'/\omega$, we have

$$A_m(\tau)=e^{(\overline{\lambda_m}t_c-\kappa/2)\omega\tau}Q_m(\tau),$$

from which we have an expression for the desired Floquet exponent for the Fourier coefficients,

$$(\lambda_m t_c)=\left(\overline{\lambda_m}t_c-\frac{\kappa}{2}\right)\omega. \tag{14}$$

It remains to find a functional form for $(\lambda_m t_c)$.

We substitute Eq. (13) into Eq. (11) to get a differential equation for the Q_m,

$$\frac{d^2Q_m}{d\tau'^2}+2(\overline{\lambda_m t_c})\frac{dQ_m}{d\tau'}+\left[\nu_m-\frac{\kappa^2}{4}+(\overline{\lambda_m}t_c)^2+\gamma\cos\tau'\right]Q_m=0.$$

We use the standard Lindstedt perturbation technique [28] for small $\gamma=1/\omega^2\beta_c$ and arrive at the following expression for $\overline{\lambda_m t_c}$:

$$\overline{\lambda_m}t_c=\pm i\pm\sqrt{\frac{\kappa^2}{4}-\nu_m}.$$

The expression for the desired Floquet exponent then is

$$\lambda_m t_c=\pm i\omega\pm\sqrt{\omega^2\left(\frac{\kappa^2}{4}-\nu_m\right)}-\frac{\omega\kappa}{2}.$$

Using the definitions of κ and ν_m gives

$$\lambda_m t_c = \pm i\omega \pm \sqrt{\frac{1}{4\beta_c^2} - \frac{\omega_m^2}{\beta_c}} - \frac{1}{2\beta_c}. \tag{15}$$

Since stability of phase locking is signaled by $\mathrm{Re}(\lambda_m t_c) < 0$, we are interested in the real part of Eq. (15), which is

$$\mathrm{Re}(\lambda_m t_c) = -\frac{1}{2\beta_c} \pm \mathrm{Re}\left[\frac{1}{2\beta_c}\sqrt{1-4\beta_c\omega_m^2}\right]. \tag{16}$$

This result will be compared with the numerical results for the Floquet exponents from the RCSJ model. Some comments about Eq. (16) are in order. Note that all factors of the angular frequency have canceled out. In fact, it can be shown that in this formalism [20] $\omega = i_B$ or $T/t_c = 2\pi/i_B$, and indeed we have checked numerically that the period of the voltages across the horizontal junctions satisfies this simple expression very well over a wide range of bias currents. Thus we have a simple way to keep track of the angular frequency; it is merely equal to the numerical value of the bias current. Equation (16) implies that the Floquet exponents should be independent of the bias current, as is indeed observed in Fig. 4.

Note that Eq. (16) can also provide the Floquet exponents for a single junction, which follow by simply taking the limit as $\Lambda \to 0$. Such a limit physically corresponds to zero coupling between neighboring junctions. In this case we of course lose the phonon modes, $\omega_m \to 0$, and Eq. (16) gives the two values of zero and $-1/\beta_c$ for the exponent. Based on Fig. 2, we see that over a wide range of junction capacitances, specifically $\beta_c > \beta_c^*(N)$, the minimum nonzero exponent for the array, $-1/2\beta_c$, is one-half that of a single junction. Furthermore, for $\beta_c < \beta_c^*(N)$, the effects of the $m=1$ mode (see Sec. IV) of the array are to reduce the magnitude of the decay rate even further below that of a single junction.

The issue of the stability to solutions of Mathieu's equation has been well studied, and the results are presented in a so-called stability diagram [28]. If the generic Mathieu equation has the form $d^2x/dt^2 + (F + G\cos t)x = 0$, then the stability diagram is just a representation, in the F-G plane, of those values of F and G for which stable solutions exist. The work of van der Zant and collaborators [13,14], as mentioned previously, studied instabilities of the whirling mode solutions near one of the so-called Mathieu tongues, in the neighborhood of the point $F = 1/4$ and $G = 0$. Comparing our Eq. (11) with the generic Mathieu equation we make the observations that

$$F = \frac{\omega_m^2}{\omega^2\beta_c} - \frac{1}{4\beta_c^2\omega^2}, \quad G = \frac{1}{\omega^2\beta_c}. \tag{17}$$

Using values typical of our numerical simulations, for example $\omega = 5$, $\beta_c = 10$, and $N = 10$, would give a value of $G = 0.004$. To have an *unstable* whirling solution, we would need the value of F to be approximately 1/4. Plugging this number into Eq. (17) then yields $\omega_m = 7.91$. Given that the functional form of the normal mode frequencies is $\omega_m = 2\Lambda \sin(m\pi/N)$, and considering the long-wavelength mode $m=1$ [35], gives us an approximate value for the critical current anisotropy needed for an unstable whirling mode solution. One gets $\Lambda = 18$, which corresponds to $I_{cy}/I_{cx} = 648$. We have not performed simulations with such a high degree of anisotropy (or with such a large nearest-neighbor junction coupling). Our typical values for Λ, namely $0.1 \leq \Lambda \leq 2$, places us nearer to the origin of the stability diagram, which is in a region of *stable* phase-locked solutions, than it does to the point $F = 1/4$, $G = 0$.

We see that our analytic result for the Floquet exponent, Eq. (15), which follows from a straightforward perturbation method, is nearly the same form as that for the decay constant of a damped, harmonic oscillator with damping constant $1/\beta_c$ and characteristic angular frequency $\omega_0^2 = \omega_m^2/\beta_c$. The only difference is the imaginary term $\pm i\omega$. That such a simple analytic result should be obtained is perhaps surprising, but it can hopefully offer us some physical insight into the dynamics of the ladder, as we discuss in the next section. One could, in principle, use the Lindstedt method to calculate λ_m to the next higher order in γ. The resultant expression should, of course, deviate from Eq. (15) by a small amount. It is not clear if such a calculation is worthwhile.

IV. DISCUSSION

Consider the set of all possible exponents resulting from Eq. (16) when the normal mode index runs over its range, $0 \leq m \leq N-1$. For the $m=0$ mode, we see that the two possible values are $\mathrm{Re}(\lambda_0 t_c) = 0, -1/\beta_c$, where in fact $-1/\beta_c$ is the largest possible magnitude exponent one can obtain from Eq. (16) and represents the fastest decaying mode of the array. (As mentioned in Sec. III these are just the Floquet exponents for a single junction.) For all modes $m > 0$, the possible exponents can be divided into two categories, depending on whether the argument of the square root in Eq. (16) is less than or greater than zero. We shall refer to the case of when the argument of the square root is less (greater) than zero as the ''overdamped'' (''underdamped'') regime. Thus we have

$$\mathrm{Re}(\lambda_m t_c) = \begin{cases} -\dfrac{1}{2\beta_c} & \text{if} \quad 4\beta_c\omega_m^2 > 1 \\ -\dfrac{1}{2\beta_c}\left[1 \pm \sqrt{1-4\beta_c\omega_m^2}\right] & \text{if} \quad 4\beta_c\omega_m^2 < 1. \end{cases} \tag{18}$$

Figure 7 offers a comparison of the numerical (RCSJ) and analytic (DSG) results for the Floquet exponents for several array sizes and zero external field. The analytic results, shown as line plots, were obtained by plotting, for a given β_c and N, the exponent from Eq. (18) with the *smallest magnitude*. For a given N we see from the figure that the two models give $\mathrm{Re}(\lambda_{min}) = -1/2\beta_c$ over an appreciable range of β_c values. The quantitative agreement fails in the region of the crossover value, $\beta_c^*(N)$, from underdamped to overdamped behavior. However, the two models are in qualitative agreement in that they both show that a crossover indeed occurs. In the case of the DSG equation, the crossover observed in Fig. 7 (for all values of N shown) results from the long-wavelength phonon mode, $m=1$, making the change from underdamped to overdamped dynamics as β_c is decreased. In essence, below the crossover, the longest-

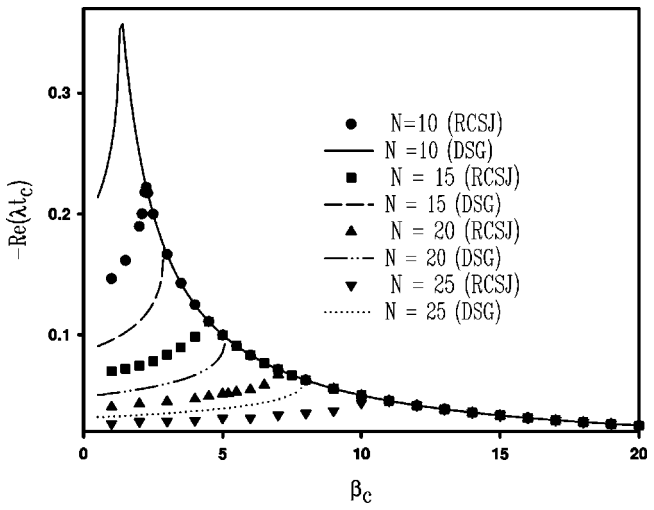

FIG. 7. Magnitude of the minimum Floquet exponent versus the McCumber parameter for four different ladder sizes. The plots show the results for both the resistively and capacitively shunted junction (RCSJ) model and discrete sine-Gordon (DSG) equation. For a given ladder size, there is quantitative agreement between the two models for a reasonable range of β_c values, and both models show nonmonotonic behavior, with a maximum value that is dependent on ladder size. The lack of quantitative agreement for all values of β_c shown reflects the different physics inherent in the models and the fact that that difference becomes more pronounced at small β_c.

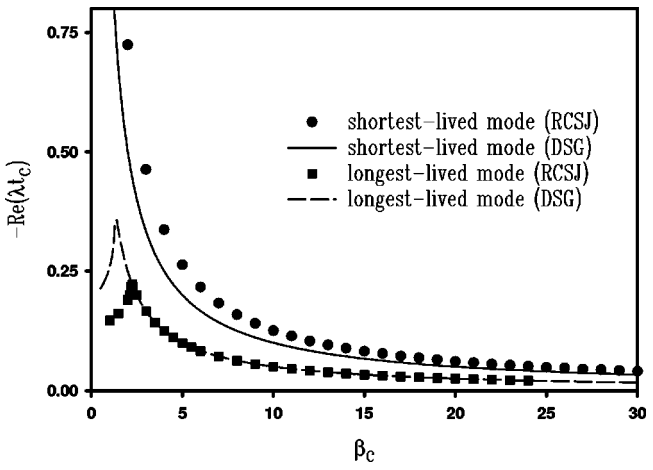

FIG. 8. Magnitude of both the minimum and maximum Floquet exponent versus the McCumber parameter for an $N=10$ ladder with $i_B=10$ and $\Lambda=1/\sqrt{2}$. The minimum (maximum) exponent corresponds to the longest-lived (shortest-lived) mode of the array. The results from both the RCSJ model and DSG equation are shown. Both models show a monotonic increase in the exponent as β_c is decreased for the shortest-lived mode. This may be due to the fact that the dynamics driving this mode have not crossed over from underdamped to overdamped behavior. The results for the longest-lived mode are the same as in Fig. 7.

wavelength phonon mode has become less effective at damping out perturbations. As a result, for $\beta_c<\beta_c^*(N)$, the smallest magnitude exponent decreases as β_c decreases. Figure 7 also shows that the DSG equation consistently predicts the crossover to occur at a value of the McCumber parameter that is smaller than that from the numeric results.

From the analytic results it is easy to see that the crossover point, $\beta_c^*(N)$, increases as N increases. The crossover results when the square root in Eq. (16) vanishes, i.e., when

$$\beta_c^*(N)=\frac{1}{4\omega_m^2}.$$

Clearly, for any value of m, ω_m decreases as N increases, and thus $\beta_c^*(N)$ should increase. Physically, as the ladder length increases, why doesn't it take as much damping *per junction* for the longest-lived mode to crossover to overdamped behavior? Simply put, the more junctions one has available the more elements in the array there are absorbing energy. Thus each junction does not have to absorb as much energy to have the same overall effect on the damping in the ladder as in a shorter array. Note, also, that our analytic result tells us that in the limit of an infinitely long ladder the crossover point $\beta_c^*(N)$ also approaches infinity. In such a limit, evidently, all the modes of the ladder must be considered to be in the overdamped regime.

It is interesting to consider the limit of Eq. (18) for $\beta_c\rightarrow 0$. One finds $Re(\lambda_m t_c)=-\omega_m^2$ in this limit. For the values $m=1$ and $N=10$, say, a quick check of Fig. 7 shows that the analytic result does indeed approach the expected value, i.e., $-\omega_1^2$. It is also clear that the corresponding results from the RCSJ model are approaching a finite value less than the DSG result as $\beta_c\rightarrow 0$. It would be of interest to calculate the Floquet exponents for the RCSJ model numerically in the overdamped ($\beta_c\rightarrow 0$) regime.

We would like to emphasize that, even though the results based on the DSG equation do not quantitatively agree with those from the RCSJ model for all β_c values shown in the figure, the DSG work is worthwhile for a couple of reasons. The fact that both models show the crossover behavior *at all* seems to suggest that they carry similar physics. One might indeed have feared that in the small β_c limit (say, $\beta_c\lesssim 2$) the two models might have differed even more than Fig. 7 shows. Also, the analytic result, with its overdamped and underdamped regimes, offers a simple way to think about the physics of the array that hopefully offers some insight into the dynamics of the RCSJ model as well.

Figure 8 simply shows that, for $N=10$, $i_B=10$, and $\Lambda=1/\sqrt{2}$ the analytic and numerical results are in reasonable agreement for the shortest-lived mode of the array (with a stability determined by what we could call λ_{max} as opposed to λ_{min}) over an even larger range of β_c values than for the longest-lived mode. This could be due to the fact that the shortest-lived ladder modes are dependent on the higher frequency lattice normal modes, the ω_m with $m>1$. These higher frequency normal modes simply have not made the crossover from underdamped to overdamped behavior for the values of β_c shown in the figure. In fact, for the values of N and Λ used to produce the plots in Fig. 8, the DSG equation would predict the $m=2$ mode to crossover at a McCumber parameter of 0.36, clearly smaller than the smallest β_c used in the simulations.

Figure 9 compares $\mathrm{Re}(\lambda_{min}t_c)$ for the two models as a function of the critical current anisotropy for a fixed damping of $\beta_c=20$. Based on Eq. (18) and the fact that $\omega_m=2\Lambda\sin(m\pi/N)$, we see that tuning the anisotropy can affect the crossover from underdamping to overdamping. Analyti-

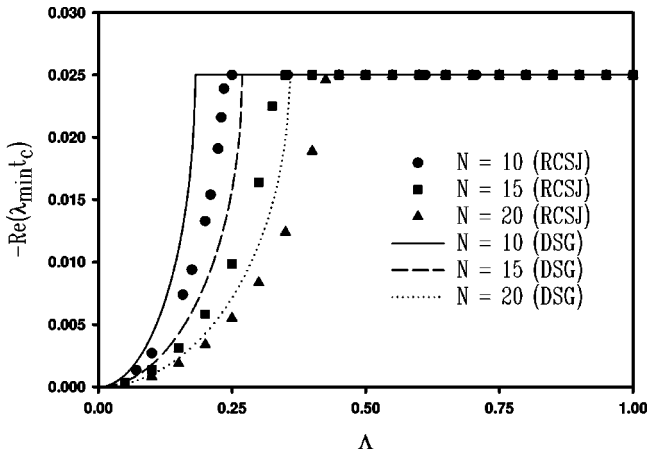

FIG. 9. Magnitude of the minimum Floquet exponent versus critical current anisotropy for three different ladder sizes. The McCumber parameter was $\beta_c=20$, and the dc bias current was $i_B=10$. Shown are results both for the RCSJ and DSG models.

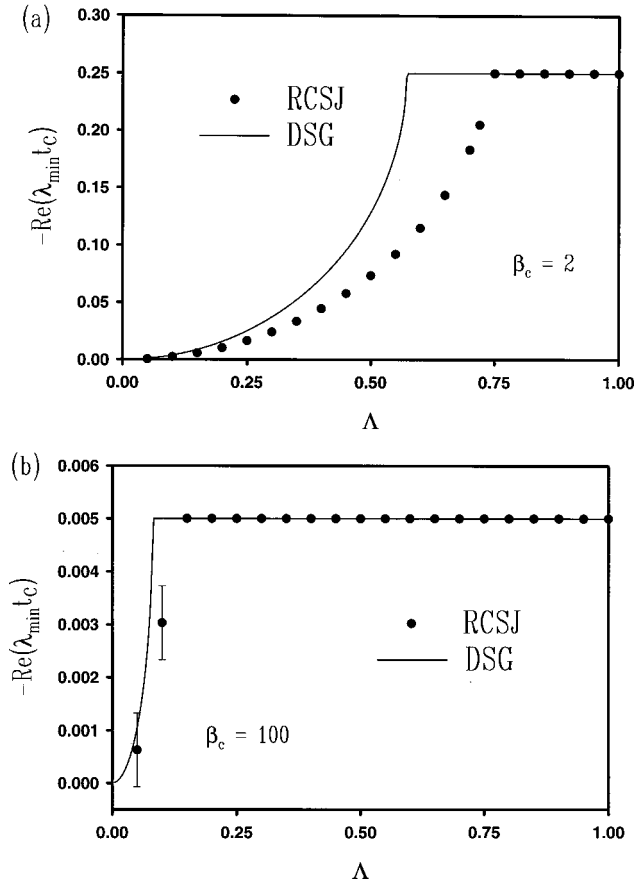

FIG. 10. Magnitude of the minimum Floquet exponent versus critical current anisotropy for an $N=10$ ladder and $i_B=10$. Results are shown for both the RCSJ and DSG models. (a) corresponds to $\beta_c=2$. We would expect a larger discrepancy between the two models for the case of smaller β_c. (b) corresponds to $\beta_c=100$. The error bars on the results from the RCSJ model for the smallest two values of Λ are a consequence of the fact that the numerical value of the exponent is a weakly periodic function of the run time of the computer code. Those two data points represent an average over many different run times, and the error bars give the standard deviation of the average of the results.

cally, such a crossover should occur at

$$\Lambda^*(N)=\sqrt{\frac{1}{16\beta_c\sin^2\left(\frac{m\pi}{N}\right)}}. \tag{19}$$

This result makes it clear, mathematically, why the crossover increases as N increases, as is clearly observed in the figure. And above the crossover, of course, we have $\mathrm{Re}(\lambda_{min}t_c)=-1/2\beta_c$, independent of Λ, as expected. As discussed with respect to Fig. 5, physically one expects $\lambda_{min}\to 0$ as $\Lambda\to 0$. Mathematically, we can see from Eq. (18) why this behavior is observed. As $\Lambda\to 0$ clearly $4\beta_c\omega_m^2<1$ and the square root approaches unity. Thus we have $\mathrm{Re}(\lambda_m)\to -1/2\beta_c\pm 1/2\beta_c$, of which zero is one possible result. The other possible result is $-1/\beta_c$, which represents the exponent for the shortest-lived mode.

Figure 10 shows the Floquet exponent's dependence on Λ for two widely different values of β_c. The larger discrepancy between analytic and numerical results would be expected for the case of the smaller β_c. The analytic result is easy to understand from Eqs. (18) and (19). The error bars on the numerical results for $\beta_c=100$ arise because of an interesting effect, which is presumably due to the low damping per junction ($\beta_c=100$) and the low coupling between junctions ($\Lambda\approx 0.2$). The numerical value of the exponent, in the two cases for which the error bars appear, is dependent upon how long the code runs to ''equilibrate'' the phases before the perturbation is applied that will result in the calculation of λ. As the run time before perturbing is increased steadily, for example, the numerically calculated value of λ_{min} varies smoothly back and forth between a maximum and minimum value. The results shown in Fig. 10 represent an average λ_{min} over several (around ten) different run times, and the error bars represent the standard deviation of the mean of these values. Similar behavior of the exponent, but not so

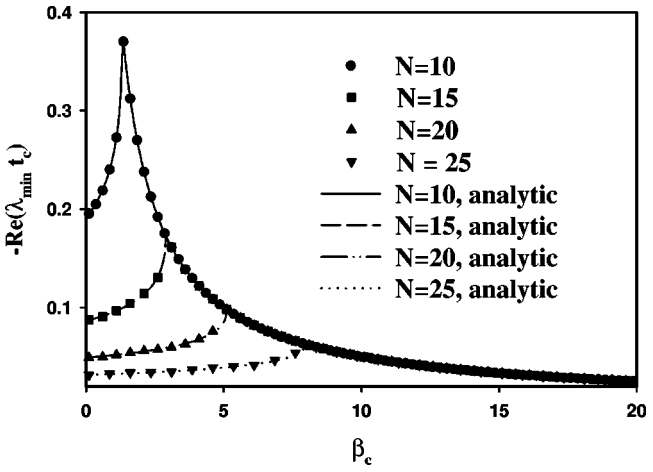

FIG. 11. A comparison of the magnitude of the minimum Floquet exponent versus the McCumber parameter as calculated for the discrete sine-Gordon equation in two different ways: analytically, based on the Lindstedt method and resulting in Eq. (16), and numerically, based on Eq. (6) directly. These results correspond to $i_B=10$, $\Lambda=1/\sqrt{2}$, and four different ladder sizes. Agreement between the two sets of solutions is excellent.

pronounced, was observed for some other values of β_c and Λ, but the resulting error bars were never larger than the size of the symbol itself.

Finally, as a useful check of our analytic results for the Floquet exponents, we have calculated the exponents *numerically* for Eq. (6) directly. Figure 11 compares the numeric and analytic results for the exponents of the DSG equation for $i_B=10$, $\Lambda=1/\sqrt{2}$, and four different ladder sizes. The agreement is clearly excellent, even for ''small'' junction capacitances, $\beta_c<1$. Equation (16) truly does describe the decay rate for perturbations to the solutions of Eq. (6) in the whirling regime, at least for the longest-lived mode of the array.

V. CONCLUSION

We have studied the dynamics of a ladder of Josephson junctions via the RCSJ model and the DSG equation. We calculated the Floquet exponents for phase locking in the horizontal junctions for a range of values of bias current, junction capacitance, and critical current anisotropy for which stable solutions to the model equations exist. We found the analytic results from the DSG equation agree quantitatively with the numerical results from the RCSJ model over a wide range of β_c and Λ values and even agree qualitatively for $\beta_c\rightarrow 1$ and $\Lambda\rightarrow 0$. The analytic result helped us to understand that perturbations to the superconducting phase differences across the horizontal junctions (whose lifetime is in essence measured by the inverse of the Floquet exponents) are damped by the small-angle oscillation (normal) modes of the lattice. And like a simple, classical harmonic oscillator with damping, each normal mode has a crossover (as a function of some parameter such as β_c or Λ) from underdamped to overdamped dynamics. Such crossover behavior is clearly visible in the plots of $\mathrm{Re}(\lambda_{min}t_c)$ versus β_c and $\mathrm{Re}(\lambda_{min}t_c)$ versus Λ. The peak in the Floquet exponent for the longest-lived ladder mode as a function of the McCumber parameter is intriguing in that it speaks of the opportunity, at least in principle, to control β_c such as to optimize the stability of the phase-locked solutions. Such a capability may be useful to applications-oriented researchers.

ACKNOWLEDGMENTS

The authors wish to thank Professor David Stroud and Professor Barbara Andereck for useful discussions. This work has been supported in part by a grant to Ohio Wesleyan University from the Howard Hughes Medical Institute Undergraduate Biological Sciences Education Program, HHMI Grant No. 71196-529503.

[1] P. Caputo, M. V. Fistul, A. V. Ustinov, B. A. Malomed, and S. Flach, Phys. Rev. B **59**, 14 050 (1999).
[2] M. Barahona, S. H. Strogatz, and T. P. Orlando, Phys. Rev. B **57**, 1181 (1998).
[3] J. J. Mazo and J. C. Ciria, Phys. Rev. B **54**, 16 068 (1996).
[4] S. Ryu, W. Yu, and D. Stroud, Phys. Rev. E **53**, 2190 (1996).
[5] I. Hwang, S. Ryu, and D. Stroud, Phys. Rev. B **53**, R506 (1996).
[6] L. M. Floría, J. L. Marín, P. J. Martínez, F. Falo, and S. Aubry, Europhys. Lett. **36**, 539 (1996).
[7] C. Denniston and C. Tang, Phys. Rev. Lett. **75**, 3930 (1995).
[8] B. J. Kim, S. Kim, and S. J. Lee, Phys. Rev. B **51**, 8462 (1995).
[9] J. M. Kim and S. J. Lee, Phys. Rev. B **50**, 13 829 (1994).
[10] J. Kim, W. G. Chee, S. Kim, and H. J. Lee, Phys. Rev. B **49**, 459 (1994).
[11] A. V. Ustinov, M. Cirillo, and B. A. Malomed, Phys. Rev. B **47**, 8357 (1993).
[12] M. Kardar, Phys. Rev. B **33**, 3125 (1986).
[13] H. S. J. van der Zant, T. P. Orlando, S. Watanabe, and S. H. Strogatz, Phys. Rev. Lett. **74**, 174 (1995).
[14] S. Watanabe, S. H. Strogatz, H. S. J. van der Zant, and T. P. Orlando, Phys. Rev. Lett. **74**, 379 (1995).
[15] A. V. Ustinov, M. Cirillo, B. H. Larsen, V. A. Oboznov, P. Carellí, and G. Rotolí, Phys. Rev. B **51**, 3081 (1995).
[16] P. J. Martínez, L. M. Floría, J. L. Marín, S. Aubry, and J. J. Mazo, Physica D **119**, 175 (1998).
[17] L. M. Florí, J. L. Marín, S. Aubry, P. J. Martínez, F. Falo, and J. J. Mazo, Physica D **113**, 387 (1998).
[18] J. J. Mazo, F. Falo, and L. M. Floría, Phys. Rev. B **52**, 10 433 (1995).
[19] J. F. Currie, S. E. Trullinger, A. R. Bishop, and J. A. Krumhansl, Phys. Rev. B **15**, 5567 (1977).
[20] S. Watanabe, H. S. J. van der Zant, S. H. Strogatz, and T. P. Orlando, Physica D **97**, 429 (1996).
[21] H. S. J. van der Zant, M. Barahona, A. E. Duwel, E. Trías, T. P. Orlando, S. Watanabe, and S. H. Strogatz, Physica D **119**, 219 (1998).
[22] L. M. Floría and J. J. Mazo, Adv. Phys. **45**, 505 (1996).
[23] S. N. Coppersmith and D. S. Fisher, Phys. Rev. B **28**, 2566 (1983), and references therein.
[24] Z. Zheng, B. Hu, and G. Hu, Phys. Rev. E **57**, 1139 (1998), and references therein.
[25] Y. Frenkel and T. K. Kontorova, Zh. Eksp. Teor. Fiz. **8**, 1340 (1938).
[26] This is for the classical limit, where the charging energy of the junction is much less than the Josephson tunneling energy.
[27] Z. Q. Wang and D. Stroud, Phys. Rev. B **44**, 9643 (1991).
[28] D. W. Jordan and P. Smith, *Nonlinear Ordinary Differential Equations* (Clarendon, Oxford, 1977).
[29] If *any* exponents are positive, then phase locking in the ladder, for the given values of bias current, capacitance, and critical current anisotropy, is not stable because perturbations grow with time. We do not find any evidence for such an instability for the values of these parameters that we have used.
[30] See, for example, J. B. Marion and S. T. Thornton, *Classical Dynamics of Particles and Systems* (Saunders, Fort Worth, 1995), pp. 116–123.
[31] B. R. Trees and D. Stroud, Phys. Rev. B **59**, 7108 (1999).
[32] These arrays are similar to that of Fig. 1, except that there are no vertical junctions, just superconducting shorts connecting the horizontal junctions.
[33] These ''phonons'' can be thought of as small-angle oscilla-

tions, or normal modes, of the pendulum system. They have also been described as phasons or spin-wave-like modes of the junction arrays.

[34] See Ref. [4] for the derivation of the DSG equation from the RCSJ model.

[35] As will be seen in Sec. IV, the long-wavelength normal modes seem to play an important role in determining the Floquet exponent for the longest-lived mode of the ladder.